Chinese Physics Letters

LETTER

Hybrid Optomechanical Cooling with Kerr Magnons and Squeezed Vacuum

Cite as: Xiao-Hong Fan *et al*. 2026 *Chin. Phys. Lett.* **43** 090705

DOI CSTR

Recommended Articles

Sub-Doppler Laser Cooling of ^{23}Na in Gray Molasses on the D_{2} Line
Zhenlian Shi, Ziliang Li, Pengjun Wang, Zengming Meng, Lianghui Huang, and Jing Zhang
Chin. Phys. Lett. **35**, 123701 (2018)

Laser Cooling Alkaline-earth Atoms for Optical Clock in Chinese Space Station
Guodong Zhao *et al*.
Chin. Phys. Lett. **42**, 063701 (2025)

Production of Degenerate Fermi Gases of ^{6}Li Atoms in an Optical Dipole Trap
Xiang-Chuan Yan, Da-Li Sun, Lu Wang, Jing Min, Shi-Guo Peng, and Kai-Jun Jiang
Chin. Phys. Lett. **38**, 056701 (2021)

Optimized Degenerate Bose–Fermi Mixture in Microgravity: DSMC Simulation of Sympathetic Cooling
LUAN Tian, JIA Tao, CHEN Xu-Zong, and MA Zhao-Yuan
Chin. Phys. Lett. **31**, 043401 (2014)

A series journal of Chinese Physical Society distributed by IOP Publishing

Chinese Physics Letters

Chin. Phys. Lett. **43** 090705 (2026)

LETTER

DOI: 10.1088/0256-307X/43/9/090705
CSTR: 32039.14.0256-307X.43.9.090705

Hybrid Optomechanical Cooling with Kerr Magnons and Squeezed Vacuum

Xiao-Hong Fan[1], Qin-Geng Chen[1], Jiaojiao Chen[1,*], and Wei Xiong[1,2,*]

[1]Department of Physics, Wenzhou University, Wenzhou 325035, China
[2]International Quantum Academy, Shenzhen 518048, China

[*]Corresponding authors. Email: jjchenphys@wzu.edu.cn; xiongweiphys@wzu.edu.cn

Ground-state cooling is essential for accessing the quantum regime and enabling quantum control of macroscopic systems. However, achieving optomechanical cooling in the unresolved-sideband regime, where the mechanical frequency ω_b is smaller than the cavity linewidth κ, remains challenging. In this Letter, we propose an efficient cooling strategy based on a hybrid optomechanical system incorporating a yttrium iron garnet (YIG) sphere embedded in an optomechanical cavity. Under strong cavity driving, the Kerr nonlinearity of the magnons hosted in the YIG sphere gives rise to a two-magnon process. Adiabatic elimination of the magnons yields an effective two-photon process in the cavity, which destructively interferes with backaction-heating channels, surpassing the quantum backaction limit and enabling *complete suppression* of heating under optimal conditions, even in the deeply unresolved sideband regime, i.e., $\omega_b \ll \kappa$. Moreover, injecting squeezed vacuum noise into the cavity not only preserves these advantages but also delivers additional enhancements, including higher net cooling rates, reduced optomechanical coupling requirements, and improved noise robustness. Comparative analysis shows that our approach outperforms existing schemes without Kerr magnons, underscoring the potential of integrating nonlinear magnonics with optomechanics for quantum control of macroscopic mechanical systems.

Introduction

Quantum control of macroscopic objects remains a long-standing pursuit in quantum science [1,2], where cooling plays a central role in suppressing thermal motion and revealing quantum phenomena. Mechanical resonators operating in the quantum regime [3,4] have emerged as promising platforms for quantum information [5–8], quantum-limited measurements [9–14], and fundamental tests of quantum mechanics [15–18]. In cavity optomechanics, ground-state cooling can be achieved by red-sideband driving [19,20] and has been experimentally demonstrated [21–26]. However, quantum backaction limits the minimum phonon occupancy, making ground-state cooling particularly challenging in the unresolved-sideband regime (USR: $\omega_b < \kappa$). Various strategies have been proposed to overcome this limitation, including pulsed driving [27,28], dissipative coupling [29–31], squeezed driving [32], feedback control [33,34], and hybrid schemes [35–40].

With the rise of quantum materials, magnons, i.e., collective spin excitations [41], in yttrium iron garnet (YIG) spheres have attracted considerable attention owing to their high spin density and tunability [42,43]. In particular, magnon Kerr nonlinearity, originating from magnetocrystalline anisotropy [44] and experimentally realized in YIG spheres [45,46], enables diverse nonlinear phenomena, including bistability [45–48], nonreciprocal entanglement [49,50], strong spin coupling [51,52], blockade [53,54], quantum phase transitions [55,56], steady-state squeezing [57], and other nonlinear effects [58]. Here, we exploit this nonlinearity to develop an efficient cooling scheme based on a micron-sized YIG sphere embedded in an optomechanical cavity. Under strong cavity driving, the magnon Kerr nonlinearity induces a two-magnon process that, after adiabatic elimination of the magnon mode, becomes an effective two-photon process in the cavity. When the cavity couples to a thermal bath [59], this induced two-photon interaction can destructively interfere with the backaction-heating channel, thereby overcoming the sideband-resolution constraint imposed by quantum backaction and enabling ground-state cooling in the USR. Under optimal cooling conditions, backaction heating is fully suppressed, yielding a significantly reduced minimum phonon occupancy.

Table 1. Abbreviations and Definitions.

Abbreviation	Definition
YIG	Yttrium iron garnet
USR	Unresolved sideband regime
DUSR	Deeply unresolved sideband regime
SB	Sideband cooling scheme
KS	Kerr-magnon cooling scheme
SS	Squeezed cooling scheme
HS	Hybrid cooling scheme

Moreover, injecting squeezed vacuum into the cavity further enhances the cooling performance under these conditions, providing higher net cooling rates, lower optomechanical coupling requirements, and greater robustness against noise. By optimizing the two-photon interaction strength, our scheme can outperform both standard sideband cooling (SB) [19] and squeezed cooling (SS) [32, 60]. Thus, our work provides a route to quantum control of macroscopic mechanical systems by combining Kerr magnonics with optomechanics.

Our scheme is conceptually related to parametrically assisted bad-cavity cooling [61], as both employ an effective two-photon process to suppress the backaction-heating channel. The key difference lies in its physical origin: in Ref. [61], the two-photon process is generated by parametric driving of the cavity, whereas in our scheme it originates from the magnon Kerr nonlinearity and emerges in the cavity through adiabatic elimination. Asjad *et al.* [62] also exploit magnon Kerr nonlinearity to suppress Stokes scattering (i.e., backaction), but their magnon mode directly couples to the mechanical mode, unlike our magnon-mediated mechanism. Zoepfl *et al.* [63] exploit intrinsic cavity Kerr nonlinearity to reshape the cavity response, while Yang *et al.* [64] use magnon thermal noise as an incoherent drive to enhance photon-phonon coupling. These distinctions highlight the distinct physical mechanism of our approach, based on magnon-Kerr-induced

Received 18 May 2026; accepted 17 August 2026; published 8 September 2026
© 2026 Chinese Physical Society and IOP Publishing Ltd. All rights, including for text and data mining, AI training, and similar technologies, are reserved.

Check for updates

two-photon interference.

The cavity mode in our scheme actually not only provides dissipation channels for phonons, but also acts as an interface for the interference between the two-photon process and backaction-heating channels, enabling cooling in the USR. Besides, the cavity also provides a convenient interface for injecting squeezed vacuum to further enhance cooling. Since adiabatic elimination is crucial for the two-photon process, a large magnon-photon coupling is detrimental for cooling in the USR [60]. To facilitate reading, the abbreviations used in this article are listed in Table 1.

The Model and Hamiltonian

We consider a hybrid quantum system comprising a micron-sized YIG sphere embedded in a driven optomechanical cavity with frequency ω_a [see Fig. 1(a)]. In a rotating frame at the drive frequency ω_d, the total Hamiltonian is given by (setting $\hbar = 1$) $H = H_{OM} + H_K + H_I + H_D$, where $H_{OM} = \delta_a a^\dagger a + \omega_b b^\dagger b + g_0 a^\dagger a(b + b^\dagger)$ is the Hamiltonian of the simplest optomechanical system, with $\delta_a = \omega_a - \omega_d$ the cavity-drive detuning, ω_b the mechanical frequency, a (b) and $a^\dagger$ ($b^\dagger$) the photon (phonon) annihilation and creation operators, and g_0 the single-photon optomechanical coupling strength. The second term, $H_K = \delta_m m^\dagger m - (K/2)m^\dagger m^\dagger mm$, is the Hamiltonian of Kerr magnons, where $\delta_m = \omega_m - \omega_d$ with ω_m the magnon frequency is the magnon-drive detuning, m ($m^\dagger$) is the magnon annihilation (creation) operator, and K characterizes the strength of the Kerr nonlinearity, arising from the magnetocrystalline anisotropy, which can be well controlled by the static magnetic field B_0 [45,46]. The third term, $H_I = J(a^\dagger m + am^\dagger)$, captures the photon-magnon interaction, with coupling strength J. The last term, $H_D = \varepsilon_d(a^\dagger + a)$, models a coherent field, with ε_d being the drive amplitude. For a strong drive, the system can be linearized around its steady state, leading to frequency shifts on both the cavity mode and the Kittel mode [see the Supplementary Material (SM) [65] for details], i.e., $\Delta_a = \delta_a + g_0(b_s + b_s^*)$ and $\Delta_m = \delta_m - 2K|m_s|^2$, with b_s and m_s steady-state values. Additionally, the optomechanical coupling is correspondingly enhanced to $G = g_0 a_s$ and the Kerr nonlinearity is transformed into a two-magnon process ($\propto m^\dagger m^\dagger + mm$) with tunable coefficient $K_m = Km_s^2$ [65]. By adiabatically eliminating the degrees of freedom of the rapidly decohering Kerr magnons, the effective optomechanical Hamiltonian can be obtained [65],

$$H_{\rm eff} = \Delta a^\dagger a + \omega_b b^\dagger b + G(a + a^\dagger)(b + b^\dagger) + H_{A^2}, \tag{1}$$

where $\Delta = \Delta_a - \eta\Delta_m$ is the effective frequency of the cavity with the effective decay rate $\kappa = \kappa_a + \eta\kappa_m$, with $\eta = J^2/(\Delta_m^2 + \kappa_m^2/4 - |K_m|^2)$. The last term, $H_{A^2} = \xi^* a^2 + \xi a^{\dagger 2}$ with $\xi = -\eta K_m/2$, represents the two-photon process induced by Kerr magnons.

Optomechanical Cooling with Kerr Magnons

When Kerr magnons are introduced (i.e., $\xi \neq 0$), we term the scheme as Kerr-magnon cooling scheme (KS). In the weak-coupling regime ($G \ll \kappa$), the radiation-pressure spectrum is given by [65]

$$V_{KS}(\omega) = \frac{V_{SB}(\omega)|1 - 2i\xi\chi(-\omega)|^2}{|1 - 4|\xi|^2\chi(\omega)\chi^*(-\omega)|^2}, \tag{2}$$

where $V_{SB}(\omega) = G^2\kappa x_{ZPF}^2|\chi(\omega)|^2$ is the spectrum of SB, $\chi(\omega) = [\kappa/2 - i(\omega - \Delta)]^{-1}$ is the cavity susceptibility, and $x_{ZPF} = \sqrt{\hbar/(2m_{eff}\omega_b)}$ is the zero-point fluctuation amplitude of the mechanical oscillator with effective mass m_{eff}. According to Fermi's golden rule [66], the cooling and heating rates are defined as $\Gamma_{KS}^- = x_{ZPF}^2 V_{KS}(\omega_b)$ and $\Gamma_{KS}^+ = x_{ZPF}^2 V_{KS}(-\omega_b)$, respectively. The net cooling rate is then given by

$$\Delta\Gamma_{KS} = \Gamma_{KS}^- - \Gamma_{KS}^+ = \frac{|1 - 2i\xi\chi(-\omega_b)|^2\Gamma_{SB}^- - |1 - 2i\xi\chi(\omega_b)|^2\Gamma_{SB}^+}{|1 - 4|\xi|^2\chi(-\omega_b)\chi^*(\omega_b)|^2}, \tag{3}$$

where $\Gamma_{SB}^- = x_{ZPF}^2 V_{SB}(\omega_b) = G^2\kappa/[\kappa^2/4 + (\omega_b - \Delta)^2]$ and $\Gamma_{SB}^+ = x_{ZPF}^2 V_{SB}(-\omega_b) = G^2\kappa/[\kappa^2/4 + (\omega_b + \Delta)^2]$ are the cooling and heating rates in SB. Figure 2(a) shows the normalized radiation-pressure spectrum for the SB and KS schemes. In the SB scheme, the cooling sideband ($\omega = \omega_b$) and the heating sideband ($\omega = -\omega_b$) differ only slightly in the USR, so the Stokes heating cannot be effectively suppressed. In the KS scheme, the two-photon process induced by Kerr magnons introduces a new heating path. The cavity susceptibility at the heating sideband no longer originates only from the linear backaction-heating channel, but includes two quantum paths: (i) Backaction-heating path induced by cavity dissipation; (ii) Parametric amplification conversion paths generated by two-photon process induced by Kerr magnons. The two paths interfere at the Stokes sideband, producing destructive quantum interference, thus suppressing the heating process. Notably, at $\omega = -\omega_b$, destructive interference completely suppresses the heating process, i.e., $\Gamma_{KS}^+ = x_{ZPF}^2 V_{KS}(-\omega_b) = 0$, directly giving rise to an optimal

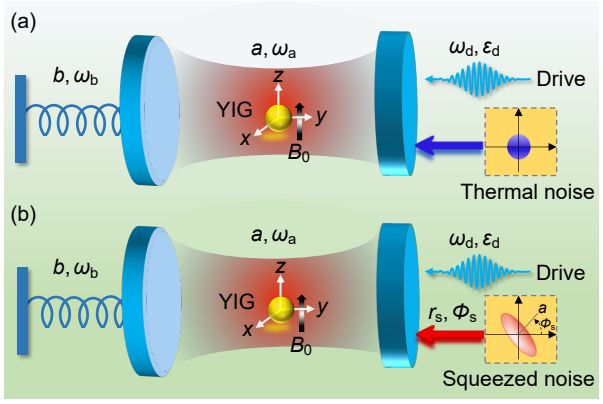

Fig. 1. Schematic diagram of the proposed hybrid quantum system. A yttrium iron garnet (YIG) sphere supporting Kerr magnons is placed inside a driven optomechanical cavity and subjected to a static magnetic field B_0 (black arrow) aligned along the crystallographic z-axis. (a) The cavity is coupled to a thermal reservoir (blue circle) with trivial (white) noise correlations. (b) The cavity is instead coupled to a broadband squeezed vacuum bath (red ellipse) with nontrivial correlations, characterized by squeezing parameter r_s and phase Φ_s. Here, ω_a, ω_b, and ω_d denote the frequencies of the cavity photons, mechanical mode, and drive, respectively, and ε_d is the amplitude of the drive field.

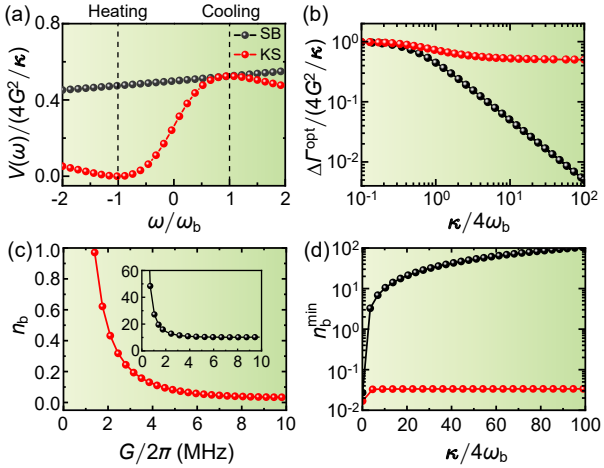

Fig. 2. (a) The normalized radiation-pressure spectra of SB (black) and KS (red) as functions of the normalized frequency ω/ω_b, with $\kappa/4\omega_b = 10$. The cooling sideband ($\omega = \omega_b$) and heating sideband ($\omega = -\omega_b$) marked by two vertical dashed lines. The corresponding cooling and heating rates are $\Gamma^- = x_{ZPF}^2 V(\omega_b)$ and $\Gamma^+ = x_{ZPF}^2 V(-\omega_b)$, respectively. (b) The normalized optimal net cooling rates of SB (black) and KS (red) as functions of the normalized cavity decay $\kappa/4\omega_b$. (c) The final phonon occupancy n_b of SB (inset) and KS (red) as functions of the coupling strength $G/2\pi$, with $\kappa/4\omega_b = 10$. (d) The minimum phonon number n_b^{min} of SB (black) and KS (red) as functions of the normalized cavity decay $\kappa/4\omega_b$. Other parameters are set as $\omega_b/2\pi = 10$ MHz, $\gamma_b/2\pi = 10$ Hz, $\Delta = \sqrt{\kappa^2/4 + \omega_b^2}$, and the thermal mean phonon number is $n_{th} = 10^3$.

cooling condition

$$\xi_{\rm KS} = \frac{\Delta - \omega_{\rm b}}{2} - {\rm i}\frac{\kappa}{4}. \tag{4}$$

When $\xi = \xi_{\rm KS}$, the net cooling rate is optimized as $\Delta\Gamma_{\rm KS}^{\rm opt} = \Gamma_{\rm SB}^{-}$ (see details in [65]). Due to unvanishing heat rate $\Gamma_{\rm SB}^{+}$, $\Delta\Gamma_{\rm KS}^{\rm opt}$ is naturally larger than the net cooling rate $\Delta\Gamma_{\rm SB}$ in SB ($\xi = 0$). Notably, $\Delta\Gamma_{\rm KS}^{\rm opt}$ is approximately enhanced by two orders of magnitude over $\Delta\Gamma_{\rm SB}$ in DUSR ($\kappa/4\omega_{\rm b} = 100$), i.e., $\Delta\Gamma_{\rm KS}^{\rm opt}/\Delta\Gamma_{\rm SB} \approx 10^2$, as shown by Fig. 2(b).

Following the quantum noise approach, the final phonon number can be expressed as $n_{\rm b} = n_{\rm c} + n_{\rm q}$, where $n_{\rm c} = n_{\rm th}\gamma_{\rm b}/\Delta\Gamma_{\rm KS}$, with mechanical damping rate $\gamma_{\rm b}$ and the thermal phonon occupation $n_{\rm th}$, denotes the classical cooling limit, and $n_{\rm q} = \Gamma_{\rm KS}^{+}/\Delta\Gamma_{\rm KS}$ represents the quantum limit. In SB, $n_{\rm q} = \kappa/4\omega_{\rm b}$ at the optimal detuning $\Delta = \sqrt{\kappa^2/4 + \omega_{\rm b}^2}$. This indicates that SB is fundamentally constrained by the sideband resolution. Therefore, SB cannot be achieved in USR [see inset in Fig. 2(c)]. However, when Kerr magnons are included, the quantum limit $n_{\rm q} = 0$ at $\xi = \xi_{\rm KS}$ because of $\Gamma_{\rm KS}^{+} = 0$. This suggests that KS is no longer constrained by the sideband resolution, enabling ground-state cooling in USR, as illustrated in Fig. 2(c). Notably, the final phonon number can be further significantly suppressed to $n_{\rm b} \ll 1$ by slightly increasing the optomechanical coupling strength G, as also demonstrated in Fig. 2(c). Figure 2(d) further reveals that the final phonon number $n_{\rm b}^{\rm min}$ at $\xi = \xi_{\rm KS}$, i.e., the minimum phonon number $n_{\rm b}^{\rm min}$, is remarkably robust against cavity dissipation when Kerr magnons are included, maintaining efficient cooling ability even in DUSR. By contrast, $n_{\rm b}^{\rm min}$ in SB is extremely sensitive to the cavity decay rate, rapidly leading to $n_{\rm b}^{\rm min} > 1$ in USR.

Hybrid Cooling with Both Kerr Magnons and Squeezed Bath

We below study hybrid cooling scheme (HS) by injecting a squeezed vacuum noise [67–70] into the optomechanical cavity including Kerr magnons [Fig. 1(b)]. Unlike thermal noise in Fig. 1(a), the squeezed noise exhibits nontrivial correlations [71]: $\langle a_{\rm in}^{\dagger}(\omega)a_{\rm in}(\omega')\rangle = \mathcal{N}_{\rm s}\delta(\omega+\omega')$, $\langle a_{\rm in}(\omega)a_{\rm in}^{\dagger}(\omega')\rangle = (\mathcal{N}_{\rm s}+1)\delta(\omega+\omega')$, $\langle a_{\rm in}(\omega)a_{\rm in}(\omega')\rangle = \mathcal{M}_{\rm s}\delta(\omega+\omega')$, and $\langle a_{\rm in}^{\dagger}(\omega)a_{\rm in}^{\dagger}(\omega')\rangle = \mathcal{M}_{\rm s}^{*}\delta(\omega+\omega')$, with $\mathcal{N}_{\rm s} = \sinh^2 r_{\rm s}$ and $\mathcal{M}_{\rm s} = {\rm e}^{-2{\rm i}\Phi_{\rm s}}\sinh r_{\rm s}\cosh r_{\rm s}$. Here, $r_{\rm s}$ and $\Phi_{\rm s}$ denote the squeezing parameter and phase, respectively. These correlations modify the radiation-pressure spectrum to

$$V_{\rm HS}(\omega) = V_{\rm KS}(\omega)\left|\cosh r_{\rm s} + A_{\xi}(\omega){\rm e}^{-2{\rm i}\Phi_{\rm s}}\sinh r_{\rm s}\right|^2, \tag{5}$$

where $A_{\xi}(\omega) = A_0(\omega)[1 + 2{\rm i}\xi^{*}\chi^{*}(\omega)]/[1 - 2{\rm i}\xi\chi(-\omega)]$ with $A_0(\omega) = \chi(-\omega)/\chi^{*}(\omega)$. Without Kerr magnons ($\xi = 0$), $A_{\xi}(\omega) = A_0(\omega)$, $V_{\rm KS}(\omega) = V_{\rm SB}(\omega)$, thus, $V_{\rm HS}(\omega) = V_{\rm SB}(\omega)|\cosh r_{\rm s} + A_0(\omega){\rm e}^{-2{\rm i}\Phi_{\rm s}}\sinh r_{\rm s}|^2 = V_{\rm SS}(\omega)$, which is just the radiation-pressure spectrum ($V_{\rm SS}$) of SS. For comparison, both $V_{\rm SS}$ (black) and $V_{\rm HS}$ (red) are plotted in Fig. 3(a). Obviously, $V_{\rm HS}(\omega)$ displays a sharp change across the frequency domain in USR ($\kappa/4\omega_{\rm b} = 10$), while $V_{\rm SS}$ nearly keeps unchanged. The abrupt variation in $V_{\rm HS}$ here is caused by the quantum interference effect, arising from the two-photon process and backaction-heating channels. This finding aligns well with the features observed in Fig. 2(a). As depicted in Fig. 3(a), the heating rate $\Gamma_{\rm HS}^{+} \propto V_{\rm HS}(\omega)$ vanishes at $\omega = -\omega_{\rm b}$, pointing to destructive interference at this frequency. This vanishing of the heat rate directly results in

$$\tanh r_{\rm s}\,{\rm e}^{-2{\rm i}\phi_{\rm s}} + A_{\xi_{\rm HS}}^{*}(\omega_{\rm b}) = 0, \tag{6}$$

which is the optimal cooling condition of HS. For SS, the optimal cooling condition is obtained by setting $\xi = 0$ in Eq. (6), yielding $\tanh r_{\rm s}{\rm e}^{-2{\rm i}\phi_{\rm s}} = -A_0^{*}(\omega_{\rm b})$. When the respective optimal conditions for two schemes are satisfied, heating processes are *completely suppressed* in both cases. As a result, the net cooling rates reach their optimal values: $\Delta\Gamma_{\rm SS}^{\rm opt} = \Delta\Gamma_{\rm SB}$ for SS and $\Delta\Gamma_{\rm HS}^{\rm opt} = \Gamma_{\rm KS}^{-}\cosh^2 r_{\rm s}$ for HS. This demonstrates that HS achieves an *exponentially enhanced* cooling rate compared to $\Gamma_{\rm KS}^{-}$ in KS, while SS can only reach the limit of SB.

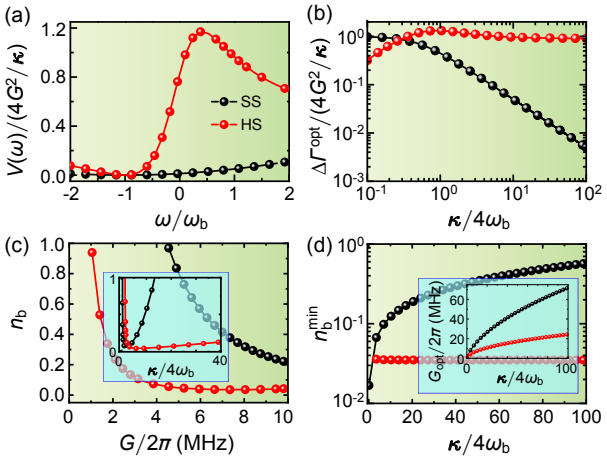

Fig. 3. (a) The normalized radiation-pressure spectra of SS (black) and HS (red) as functions of the normalized frequency $\omega/\omega_{\rm b}$, with $\kappa/4\omega_{\rm b} = 10$. (b) The normalized optimal net cooling rates of SS (black) and HS (red) as functions of the normalized cavity decay $\kappa/4\omega_{\rm b}$. (c) The final phonon occupancy $n_{\rm b}$ of SS (black) and HS (red) as functions of the coupling strength $G/2\pi$, with $\kappa/4\omega_{\rm b} = 10$. Inset: The final phonon occupancy $n_{\rm b}$ of SS (black) and HS (red) as functions of the normalized cavity decay $\kappa/4\omega_{\rm b}$, with $G/2\pi = 6$ MHz. (d) The minimum phonon number $n_{\rm b}^{\rm min}$ of SS (black) and HS (red) as functions of the normalized cavity decay $\kappa/4\omega_{\rm b}$. Inset: The optimal optomechanical coupling strength as functions of the normalized cavity decay $\kappa/4\omega_{\rm b}$, where $|\xi_{\rm HS}| = 13.92\omega_{\rm b}$. Other parameters are the same as in Fig. 2.

Unlike SS, $\Delta\Gamma_{\rm HS}^{\rm opt}$ remains nearly constant over $\kappa/4\omega_{\rm b} = 0.1$–$100$, whereas $\Delta\Gamma_{\rm SS}^{\rm opt}$ decreases rapidly [see Fig. 3(b)], demonstrating the superior cooling performance and robustness of HS in DUSR. At $\kappa/4\omega_{\rm b} = 10$, HS requires only $G/2\pi \approx 1.5$ MHz to achieve $n_{\rm b} < 1$, compared with $G/2\pi \gtrsim 4.5$ MHz for SS [Fig. 3(c)]. At fixed $G/2\pi = 6$ MHz [inset of Fig. 3(c)], HS maintains efficient cooling over the entire range $\kappa/4\omega_{\rm b} = 0.1 \sim 100$, whereas SS fails in DUSR with $n_{\rm b} \gg 1$ for $\kappa/4\omega_{\rm b} \gtrsim 10$. Consistently, $n_{\rm b}^{\rm min}$ remains nearly independent of $\kappa/4\omega_{\rm b}$ for HS but increases rapidly for SS [Fig. 3(d)]. The inset in Fig. 3(d) indicates that the required optimal coupling strength $G_{\rm opt}$ in HS is significantly smaller than that in SS.

All analytical results above are derived under the weak-coupling approximation and verified by exact master-equation simulations, as detailed in the SM [65]. Excellent agreement is found across regimes, along with a full stability analysis [72] and parameter maps for ground-state cooling. HS remains effective in DUSR and supports higher bath temperatures than other schemes, underscoring its robustness and experimental feasibility.

Cooling Enhancement via Optimization

Under the optimal cooling condition of HS given by Eq. (6), the optimal net cooling rate is achieved. However, the parameter ξ introduced in Eq. (6) remains a free variable, offering further potential for optimization. To exploit this degree of freedom, we express the parameter $\xi_{\rm HS}$ as $\xi_{\rm HS} = \xi_{\rm HS}^{\rm r} + {\rm i}\xi_{\rm HS}^{\rm i}$ and numerically explore the dependence of the net cooling rate on both the real and imaginary parts of ξ for various values of $\kappa/4\omega_{\rm b}$ [see Fig. 4(a)]. Our results demonstrate that the cooling performance can be significantly improved by jointly optimizing $\xi_{\rm HS}^{\rm r}$ and $\xi_{\rm HS}^{\rm i}$. For example, when $\kappa/4\omega_{\rm b} = 0.1$, the net cooling rate reaches an optimal value of $\Gamma_{\rm HS}^{\rm opt} = 1.36\omega_{\rm b}$ at $\xi_{\rm HS}^{\rm r} = -0.196\omega_{\rm b}$ and $\xi_{\rm HS}^{\rm i} = 0$. Similar optimizations performed across other parameter regimes yield consistently enhanced cooling rates, as summarized in the SM [65]. Remarkably, the advantage of this optimization becomes particularly pronounced in DUSR. For instance, at $\kappa/4\omega_{\rm b} = 100$, the optimized net cooling rate is enhanced by approximately three orders of magnitude compared to the unoptimized case [see the arrow in Fig. 4(b)].

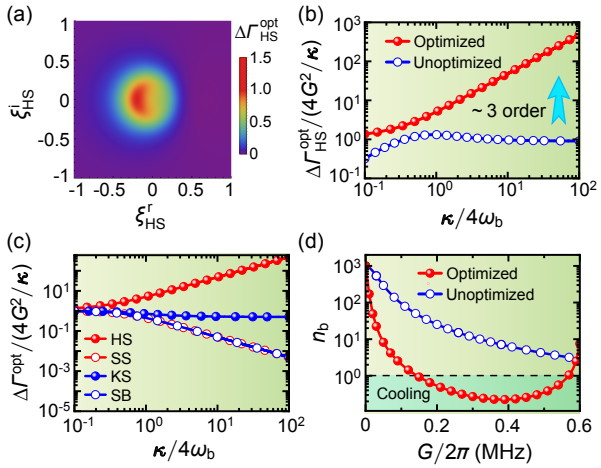

Fig. 4. (a) The optimal net cooling rate $\Delta\Gamma_{\rm HS}^{\rm opt}$ as functions of the real part ($\xi_{\rm HS}^{\rm r}$) and the imaginary part ($\xi_{\rm HS}^{\rm i}$), with ($\kappa/4\omega_{\rm b}=0.1$). (b) The unoptimized (blue) and optimized (red) net cooling rate $\Delta\Gamma_{\rm HS}^{\rm opt}$ of HS as a function of the normalized cavity decay $\kappa/4\omega_{\rm b}$. (c) The normalized net cooling rates of HS (red solid circles), SS (red open circles), KS (blue solid circles), and SB (blue open circles), as functions of the normalized cavity decay $\kappa/4\omega_{\rm b}$. (d) The phonon number $n_{\rm b}$ in HS as a function of the coupling strength $G/2\pi$ for $\kappa/4\omega_{\rm b}=10$. Blue (red) curves correspond to unoptimized (optimized) values of $\xi_{\rm HS}$. Other parameters are the same as those in Fig. 2.

To further highlight the superiority of our optimized HS, we compare its performance with SB, KS, and SS. As shown in Fig. 4(c), the optimized cooling rate in HS significantly outperforms the others, especially as the system transitions from USR ($\kappa/4\omega_{\rm b}=0.1$) to DUSR ($\kappa/4\omega_{\rm b}=100$). Specifically, while the cooling rates in SS and SB decrease, and that in KS remains nearly constant with increasing $\kappa/4\omega_{\rm b}$, the cooling rate in HS continues to grow nearly linearly. In addition to improving the cooling rate, the optimization of ξ drastically reduces the required optomechanical coupling strength to achieve efficient cooling, as shown in Fig. 4(d), with optimized $|\xi_{\rm HS}|=14.14\omega_{\rm b}$ (see the SM [65]) and $\kappa/4\omega_{\rm b}=10$, ground-state cooling is achieved with $G/2\pi\approx 0.1$ MHz, substantially below that in the unoptimized case (blue line). This reduced coupling requirement favors experimental implementation, while the white line in Fig. S4 of the SM [65] shows that the optimal coupling strength in the HS is smaller than that in the KS. These results underline the critical importance of optimizing the parameter ξ to maximize cooling efficiency, particularly in regimes where cooling in SB becomes ineffective. The pronounced enhancement underscores the potential of finely tuning the two-photon process coefficient, introduced by Kerr magnons, as a powerful and practical approach to enhance quantum control in hybrid optomechanical platforms.

Possible Implementations

The proposed protocols can be implemented in a three-dimensional (3D) electromechanical platform [73], consisting of a 3D superconducting cavity coupled to a mechanical resonator via a parallel-plate capacitor. With a typical internal volume of $\sim{\rm mm}^3$, such cavities can readily accommodate a micron-sized yttrium iron garnet (YIG) sphere, as commonly used in cavity magnonics experiments [74,75]. This makes the integration of 3D electromechanics with magnonic systems experimentally accessible using current technologies. A key requirement of our scheme is the introduction of magnon Kerr nonlinearity, which can be realized by applying a static magnetic field along specific crystallographic axes (e.g., [100] or [110]) of the YIG sphere [45,46]. High-resolution tunable electromagnets allow precise control of this static field, enabling fine-tuning of the magnonic properties. Our analysis also relies on the adiabatic elimination of the magnon mode, which requires relatively large magnon damping. This condition can be met by engineering additional losses in the YIG sphere, through either rare-earth ion doping [74] or surface deposition of iron particles to enhance scattering [75]. The required squeezed vacuum field for the 3D microwave cavity can be generated using a Josephson parametric amplifier (JPA) [32,69,70,76], a well-established technique in circuit quantum electrodynamics. JPAs enable the generation of broadband, tunable squeezed microwaves, providing the flexibility needed to optimize cooling performance as demonstrated in our work. Together, squeezed fields, Kerr magnons, and 3D optomechanics constitute a robust and accessible hybrid platform. The proposed scheme offers a realistic pathway for exploring quantum phenomena in hybrid optomechanical systems and for developing next-generation hybrid quantum devices.

Conclusion

We propose an efficient scheme for ground-state cooling in DUSR using a hybrid optomechanical system containing an embedded yttrium iron garnet (YIG) sphere. The Kerr magnons in the YIG sphere act as an auxiliary subsystem that induces effective two-photon process, enabling destructive interference with backaction-heating channels. This yields *complete suppression* of phonon heating under optimal conditions, achieving ground-state cooling in this challenging regime. By injecting squeezed vacuum noise into the cavity, we obtain additional advantages, including higher net cooling rates, reduced optomechanical coupling requirements, and improved noise resilience. Comparative analysis demonstrates that our proposal substantially advances previous schemes without Kerr magnons. These results highlight the potential of integrating nonlinear magnons with optomechanics for quantum control of macroscopic mechanical systems.

Acknowledgements

This work was supported by the National Natural Science Foundation of China (Grant No. 12605044), the Natural Science Foundation of Zhejiang Province (Grant Nos. LY24A040004 and LQN26A040020), the Zhejiang Province Key R&D Program of China (Grant No. 2025C01028), and Shenzhen International Quantum Academy (Grant No. SIQA2024KFKT010).

References

[1] Bocko M F and Onofrio R 1996 *Rev. Mod. Phys.* **68** 755
[2] Knobel R G and Cleland A N 2003 *Nature* **424** 291
[3] Kippenberg T J and Vahala K J 2008 *Science* **321** 1172
[4] Aspelmeyer M, Kippenberg T J, and Marquardt F 2014 *Rev. Mod. Phys.* **86** 1391
[5] O'Connell A D, Hofheinz M, Ansmann M *et al.* 2010 *Nature* **464** 697
[6] Verhagen E, Deléglise S, Weis S, Schliesser A, and Kippenberg T J 2012 *Nature* **482** 63
[7] Wang Y D and Clerk A A 2012 *Phys. Rev. Lett.* **108** 153603
[8] Dong C, Fiore V, Kuzyk M C, and Wang H 2012 *Science* **338** 1609
[9] LaHaye M, Buu O, Camarota B, and Schwab K 2004 *Science* **304** 74
[10] Teufel J, Donner T, Castellanos-Beltran M, Harlow J, and Lehnert K 2009 *Nat. Nanotechnol.* **4** 820
[11] McClelland D E, Mavalvala N, Chen Y, and Schnabel R 2011 *Laser Photonics Rev.* **5** 677
[12] Krause A G, Winger M, Blasius T D, Lin Q, and Painter O 2012 *Nat. Photonics* **6** 768
[13] Purdy T P, Peterson R W, and Regal C 2013 *Science* **339** 801
[14] Li B B, Bilek J, Hoff U B, Madsen L S, Forstner S, Prakash V, Schäfermeier C, Gehring T, Bowen W P, and Andersen U L 2018 *Optica* **5** 850
[15] Romero-Isart O, Pflanzer A C, Blaser F, Kaltenbaek R, Kiesel N, Aspelmeyer M, and Cirac J I 2011 *Phys. Rev. Lett.* **107** 020405
[16] Pepper B, Ghobadi R, Jeffrey E, Simon C, and Bouwmeester D 2012 *Phys. Rev. Lett.* **109** 023601
[17] Blencowe M 2013 *Phys. Rev. Lett.* **111** 021302
[18] Sekatski P, Aspelmeyer M, and Sangouard N 2014 *Phys. Rev. Lett.* **112** 080502
[19] Wilson-Rae I, Nooshi N, Zwerger W, and Kippenberg T J 2007 *Phys.*

Rev. Lett. **99** 093901
[20] Marquardt F, Chen J P, Clerk A A, and Girvin S M 2007 *Phys. Rev. Lett.* **99** 093902
[21] Gigan S, Böhm H, Paternostro M, Blaser F, Langer G, Hertzberg J, Schwab K, Bäuerle D, Aspelmeyer M, and Zeilinger A 2006 *Nature* **444** 67
[22] Arcizet O, Cohadon P F, Briant T, Pinard M, and Heidmann A 2006 *Nature* **444** 71
[23] Rocheleau T, Ndukum T, Macklin C, Hertzberg J, Clerk A, and Schwab K 2010 *Nature* **463** 72
[24] Teufel J D, Donner T, Li D, Harlow J, Allman M, Cicak K, Sirois A, Whittaker J, Lehnert K, and Simmonds R 2011 *Nature* **475** 359
[25] Chan J, Mayer Alegre T P, Safavi-Naeini A H, Hill J T, Krause A, Gröblacher S, Aspelmeyer M, and Painter O 2011 *Nature* **478** 89
[26] Peterson R, Purdy T, Kampel N, Andrews R, Yu P L, Lehnert K, and Regal C 2016 *Phys. Rev. Lett.* **116** 063601
[27] Machnes S, Cerrillo J, Aspelmeyer M, Wieczorek W, Plenio M B, and Retzker A 2012 *Phys. Rev. Lett.* **108** 153601
[28] Wang X, Vinjanampathy S, Strauch F W, and Jacobs K 2011 *Phys. Rev. Lett.* **107** 177204
[29] Elste F, Girvin S M, and Clerk A A 2009 *Phys. Rev. Lett.* **102** 207209
[30] Li M, Pernice W H P, and Tang H X 2009 *Phys. Rev. Lett.* **103** 223901
[31] Xuereb A, Schnabel R, and Hammerer K 2011 *Phys. Rev. Lett.* **107** 213604
[32] Clark J B, Lecocq F, Simmonds R W, Aumentado J, and Teufel J D 2017 *Nature* **541** 191
[33] Rossi M, Kralj N, Zippilli S, Natali R, Borrielli A, Pandraud G, Serra E, Di Giuseppe G, and Vitali D 2017 *Phys. Rev. Lett.* **119** 123603
[34] Zippilli S, Kralj N, Rossi M, Di Giuseppe G, and Vitali D 2018 *Phys. Rev. A* **98** 023828
[35] Liu Y C, Xiao Y F, Luan X, Gong Q, and Wong C W 2015 *Phys. Rev. A* **91** 033818
[36] Gu W J and Li G X 2013 *Phys. Rev. A* **87** 025804
[37] Guo Y, Li K, Nie W, and Li Y 2014 *Phys. Rev. A* **90** 053841
[38] Ojanen T and Børkje K 2014 *Phys. Rev. A* **90** 013824
[39] Chen X, Liu Y C, Peng P, Zhi Y, and Xiao Y F 2015 *Phys. Rev. A* **92** 033841
[40] Genes C, Ritsch H, and Vitali D 2009 *Phys. Rev. A* **80** 061803
[41] Stancil D D and Prabhakar A 2009 *Spin Waves* (Springer)
[42] Rameshti B Z, Kusminskiy S V, Haigh J A, Usami K, Lachance-Quirion D, Nakamura Y, Hu C M, Tang H X, Bauer G E W, and Blanter Y M 2022 *Phys. Rep.* **979** 1
[43] Yuan H Y, Cao Y, Kamra A, Duine R A, and Yan P 2022 *Phys. Rep.* **965** 1
[44] Zhang G Q, Wang Y P, and You J Q 2019 *Sci. China Phys. Mech. Astron.* **62** 987511
[45] Wang Y P, Zhang G Q, Zhang D, Luo X Q, Xiong W, Wang S P, Li T F, Hu C M, and You J Q 2016 *Phys. Rev. B* **94** 224410
[46] Wang Y P, Zhang G Q, Zhang D, Li T F, Hu C M, and You J Q 2018 *Phys. Rev. Lett.* **120** 057202
[47] Shen R C, Wang Y P, Li J, Zhu S Y, Agarwal G S, and You J Q 2021 *Phys. Rev. Lett.* **127** 183202
[48] Shen R C, Li J, Fan Z Y, Wang Y P, and You J Q 2022 *Phys. Rev. Lett.* **129** 123601
[49] Chen J, Fan X G, Xiong W, Wang D, and Ye L 2024 *Phys. Rev. A* **109** 043512
[50] Chen J, Fan X G, Xiong W, Wang D, and Ye L 2023 *Phys. Rev. B* **108** 024105
[51] Xiong W, Tian M, Zhang G Q, and You J Q 2022 *Phys. Rev. B* **105** 245310
[52] Ji F Z and An J H 2023 *Phys. Rev. B* **108** L180409
[53] Fan X H, Zhang Y N, Yu J P, Liu M Y, He W D, Li H C, and Xiong W 2024 *Adv. Quantum Technol.* **7** 2400043
[54] Hou R, Zhang W, Han X, Wang H F, and Zhang S 2024 *Phys. Rev. A* **109** 033721
[55] Zhang G Q, Chen Z, Xiong W, Lam C H, and You J Q 2021 *Phys. Rev. B* **104** 064423
[56] Liu G, Xiong W, and Ying Z J 2023 *Phys. Rev. A* **108** 033704
[57] Qi S F and Jing J 2025 *Phys. Rev. A* **111** 013708
[58] Zheng S, Wang Z, Wang Y, Sun F, He Q, Yan P, and Yuan H Y 2023 *J. Appl. Phys.* **134** 151101
[59] Walls D F and Milburn G J 2008 *Quantum Optics* (Springer)
[60] Asjad M, Zippilli S, and Vitali D 2016 *Phys. Rev. A* **94** 051801
[61] Wang H K and Clerk A A 2020 *Phys. Rev. Lett.* **124** 103602
[62] Asjad M, Li J, Zhu S Y, and You J Q 2020 *Fundam. Res.* **3** 3
[63] Zoepfl D, Juan M L, Diaz-Naufal N, Schneider C M F, Deeg L F, Sharafiev A, Metelmann A, and Kirchmair G 2023 *Phys. Rev. Lett.* **130** 033601
[64] Yang Z, Zhao C S, Peng R, Yang J Y, and Zhou L 2023 *Opt. Lett.* **48** 375
[65] See Supplemental Material for details, which includes Refs. [4,32,45,46, 59,60,66–72].
[66] Clerk A A, Devoret M H, Girvin S M, Marquardt F, and Schoelkopf R J 2010 *Rev. Mod. Phys.* **82** 1155
[67] Ast S, Mehmet M, and Schnabel R 2013 *Opt. Express* **21** 13572
[68] Serikawa T, Yoshikawa J I, Makino K, and Furusawa A 2016 *Opt. Express* **24** 28383
[69] Clark J B, Lecocq F, Simmonds R W, Aumentado J, and Teufel J D 2016 *Nat. Phys.* **12** 683
[70] Murch K W, Weber S J, Beck K M, Ginossar E, and Siddiqi I 2013 *Nature* **499** 62
[71] Breuer H P and Petruccione F 2002 *The Theory of Open Quantum Systems* (Oxford University Press)
[72] Gradshteyn I S and Ryzhik I M 1980 *Table of Integrals, Series and Products* (Academic Press)
[73] Liu Y, Sun H, Liu Q, Wu H, Sillanpää M A, and Li T 2025 *Nat. Commun.* **16** 1207
[74] Huebl H, Zollitsch C W, Lotze J, Hocke F, Greifenstein M, Marx A, Gross R, and Goennenwein S T B 2013 *Phys. Rev. Lett.* **111** 127003
[75] Zhang X, Zou C L, Jiang L, and Tang H X 2014 *Phys. Rev. Lett.* **113** 156401
[76] Castellanos-Beltran M A, Irwin K D, Hilton G C, Vale L R, and Lehnert K W 2008 *Nat. Phys.* **4** 929